High-Performance Switched Reluctance Motor Drive System Using Hysteresis-Based Pulse-Width-Modulation and Cascaded Recurrent Neural Network Controller

[1]Saritha Kandukuri, [2]Sivaprasad Kollati, [1]Sree Mohitha Garaboyina, [1]Ankit Raj, [1]Gopal Kumar

[1]School of Engineering, Godavari Institute of Engineering and Technology (A), Rajahmundry, India
[2]School of Engineering, Godavari Global University, Rajahmundry, India

Abstract. The main objectives of the study is to improve speed regulation and reduce torque ripple in Switched Reluctance Motors (SRMs), which are increasingly adopted in modern electric drive systems due to their simple construction, fault tolerance, and wide operating range. Despite these advantages, SRMs suffer from nonlinear magnetization characteristics, acoustic noise, and poor torque performance, especially under dynamic load conditions. These objectives are achieved by developing a robust and intelligent control strategy that integrates a Cascaded Recurrent Neural Network (CRNN) controller with a Hysteresis Current-Controlled (HCC) Pulse Width Modulation (PWM) generator. This hybrid control scheme is supported by a custom-designed (n+1) semiconductor and (n+1) diode power converter topology operating on a 300V DC supply, enabling precise switching and current shaping. The most important results are that the proposed CRNN-based control system exhibits accurate phase current tracking within the hysteresis band and has quick dynamic performance, achieving the reference speed of 2000 rpm in 0.06 s with a rise time of 0.03 s. Under different load circumstances, the steady-state speed error is insignificant. Furthermore, the developed control method significantly decreases torque ripple after 1 second of operation and maintains a smoother torque profile across a wide speed range of 200-2000 rpm, surpassing traditional Proportional Integral (PI) and Fuzzy Logic Controllers (FLCs). The significance of obtained results lies in demonstrating that the proposed neural-network-based control architecture improves the overall efficiency, reliability, and performance of SRMs, making them highly suitable for high-performance Electric Vehicle (EV) drives and industrial automation systems where precise speed control and minimal torque ripple are essential.
Keywords: switched reluctance motors, (n+1) semiconductor and (n+1) diode power converter, Cascaded Recurrent Neural Network, Pulse Width Modulation, and hysteresis current controller.

DOI: https://doi.org/10.52254/1857-0070.2026.1-69.03
UDC: 621.313.3

Sistem de acționarea motorului cu reluctanță comutată de înaltă performanță utilizând PWM cu histerezis și controler de rețea neuronală recurentă în cascadă

Saritha Kandukuri[1], Sivaprasad Kollati[2], Sree Mohitha Garaboyina[1], Ankit Raj[1], Gopal Kumar[1]
[1]Facultatea de Inginerie, Institutul de Inginerie și Tehnologie Godavari (A), Rajahmundry, India
[2]Facultatea de Inginerie, Universitatea Globală Godavari, Rajahmundry, India

Rezumat. Obiectivele principale ale studiului sunt îmbunătățirea reglării vitezei și reducerea fluctuațiilor de cuplu în motoarele cu reluctanță comutată (SRM), care sunt din ce în ce mai utilizate în sistemele moderne de acționare electrică datorită construcției lor simple, toleranței la erori și domeniului larg de funcționare. În ciuda acestor avantaje, SRM-urile suferă de caracteristici de magnetizare neliniare, zgomot acustic și performanțe slabe ale cuplului, în special în condiții de sarcină dinamică. Aceste obiective sunt atinse prin dezvoltarea unei strategii de control robuste și inteligente, care integrează un controler Cascaded Recurrent Neural Network (CRNN) cu un generator Hysteresis Current-Controlled (HCC) Pulse Width Modulation (PWM). Această schemă de control hibridă este susținută de o topologie personalizată (n+1) de semiconductori și (n+1) diode de conversie a puterii care funcționează cu o alimentare de 300 V c.c., permițând comutarea precisă și modelarea curentului. Controlerul CRNN procesează semnalele de eroare de viteză prin straturi convoluționale, de grupare și de activare pentru a genera impulsuri de control optimizate pentru comutatoarele convertorului, asigurând un control adaptiv și receptiv. Cele mai importante rezultate sunt că sistemul de control propus, bazat pe CRNN, prezintă o urmărire precisă a curentului de fază în banda de histerezis și are performanțe dinamice rapide, atingând viteza de referință de 2000 rpm în 0.06 s cu un timp de creștere de 0.03 s. În diferite circumstanțe de sarcină, eroarea de viteză în stare staționară este nesemnificativă. Semnificația rezultatelor obținute constă în demonstrarea faptului că

© Saritha Kandukuri, Sivaprasad Kollati,
Sree Mohitha Garaboyina,
Ankit Raj, Gopal Kumar, 2025

arhitectura de control propusă, bazată pe rețele neuronale, îmbunătățește eficiența, fiabilitatea și performanța generală a SRM-urilor, făcându-le foarte potrivite pentru acționările de înaltă performanță ale vehiculelor electrice (EV) și ale sistemelor de automatizare industrială, unde controlul precis al vitezei și ondulația minimă a cuplului sunt esențiale.

Cuvinte-cheie: motoare cu reluctanță comutată, convertor de putere cu semiconductori (n+1) și diode (n+1), rețea neuronală recurentă în cascadă, modulație a lățimii impulsurilor și controler de curent cu histerezis.

Система управления двигателем с переключаемым сопротивлением, использующая широтно-импульсную модуляцию на основе гистерезиса и каскадный контроллер на основе рекуррентной нейронной сети

Сарита Кандукури[1], Сивапрасад Коллати[2], Шри Мохита Гарабоина[1], Анкит Радж[1], Гопал Кумар[1]

[1]Институт инженерии и технологий Годавари (А), Раджамундри, Индия

[2]Глобальный университет Годавари, Раджамундри, Индия

Аннотация. Основными целями исследования являются улучшение регулирования скорости и снижение пульсаций крутящего момента в двигателях с переключаемым сопротивлением (SRM), которые все чаще используются в современных электрических приводных системах благодаря своей простой конструкции, отказоустойчивости и широкому диапазону рабочих режимов. Несмотря на эти преимущества, SRM имеют недостатки в виде нелинейных характеристик намагничивания, акустического шума и низкой величины крутящего момента, особенно в условиях динамической нагрузки. Цели исследования достигаются за счет разработки надежной и интеллектуальной системы управления, которая объединяет контроллер каскадной рекуррентной нейронной сети (CRNN) с генератором широтно-импульсной модуляции (PWM) с гистерезисным управлением током (HCC). Эта гибридная схема управления поддерживается специально разработанной топологией преобразователя мощности (n+1) полупроводников и (n+1) диодов, работающего от источника питания 300 В постоянного тока, что обеспечивает точное переключение и формирование тока. Контроллер CRNN обрабатывает сигналы ошибки скорости через слои свертки, объединения и активации для генерации оптимизированных импульсов управления для переключателей преобразователя, обеспечивая адаптивное и отзывчивое управление. Наиболее важными результатами являются то, что предлагаемая система управления на основе CRNN обеспечивает точное регулирование тока, быстрый динамический отклик и стабильное отслеживание скорости в различных условиях нагрузки и питания. Она также значительно снижает пульсации крутящего момента по сравнению с традиционными PI- или FLC-контроллерами (Fuzzy Logic Controllers), тем самым повышая плавность работы двигателя и стабильность его работы. Значение полученных результатов.

***Ключевые слова*:** двигатели с переключаемым сопротивлением, (n+1) полупроводниковый и (n+1) диодный преобразователь мощности, каскадная рекуррентная нейронная сеть, широтно-импульсная модуляция, гистерезисный регулятор тока.

I. INTRODUCTION

The advancements in EVs transportation sector demand high performance, reliability, torque density and power density, along with significant reductions in system overall cost. According to [1,2] the essential subsystems of EVs include power electronic converters, electric motors, battery packs, control strategies, structural materials, and various mechanical and electronic components many of which depend on non-earth abundant materials.

Permanent Magnet (PM) motors and Induction Motors (IM) are the dominant technologies used electric motor technology for EV's popularity at [3] due to their superior performance characteristics. However, PM motors require rare earth magnet materials such as neodymium, samarium, and iron boron while IMs rely on large quantities of copper both of which is expensive and limited in availability. These motor types also suffer from drawbacks including reduced high-speed efficiency, demagnetization risks, limited fault tolerance, high losses, low power factor issues and restricted field weakening capability [4, 5]. Consequently, researchers, industries and governments are actively pursuing alternative motor technologies that reduce dependence on rare-earth magnets [6].

As reported in [7], developments in EV powertrains are increasingly oriented toward high-power density and lower cost by adopting alternatives to magnet or copper-based intensive motors, such as wound-field synchronous machines and SRM. SRMs are magnet-free machines composed primarily low fabrication-cost silicon steel in both stator and rotor poles, offering simple construction, low fabrications cost and robustness [8, 9]. They rely on specially

designed power electronic converters to achieve improved performance and smooth operation, according to [10]. SRM's additionally provide high fault tolerance, immunity to demagnetization, resilience at high temperature, high speed operation, and robust performance under abnormal conditions [11, 12]. However, they also face challenges including torque ripple, high acoustic noise, vibration, commutation problems and moderate torque density [13, 14]. Advancements in semiconductor devices, power electronic converters, modern control strategies, are gradually mitigating these limitations and making SRMs increasingly attractive for EV drive applications [15].

A. Related work

Francisco Juarez-Leon *et al* (2025) [16] have developed a Silicon-Carbide (SiC)-based bidirectional converter topology for industrial SRM drives, demonstrating improved efficiency, reliability, and power density. However, the use of large line inductors increases overall weight and limits compactness. **Hamid Malekpour *et al* (2025) [17]** have proposed a multi-level modular converter topology for HEV SRM drive using a cascade front-end converter to provide variable DC-link voltage and enhanced drive performance. Though, high fault tolerance, and efficiency modular configuration, its complexity and dependence on multiple modules raise implementation cost and control challenges.

Qingguo Sun *et al* (2023) [18] have designed a Quasi-Z-source (QZS) converter with a four-region Direct Instantaneous Torque Control (DITC) method to reduce torque ripple, supress source current ripple, and balanced thermal stress on power devices. However, the modular QZS structure and multi-region torque control strategy significantly increase circuit and controller complexity. **Xiaodong Sun *et al* (2020) [19]** have introduced an improved Direct Torque Control (DTC), using a Sliding Mode Speed Controller (SMSC) and an Anti-disturbance Sliding Mode Observer (ADSMO). Although, it reduces torque ripple, increases response speed, and enhances anti-disturbance capability, its computational burden makes real time implementation challenging. **Benqin Jing *et al* (2022) [20]** have implemented a fuzzy Indirect Instant Torque Control (IITC) approach for a 12/8 SRM drive, This method reduces torque ripple, and simplifies control design but the computational load of fuzzy logic, limits high speed in real time application. **Diego F. Valencia *et al* (2021) [21]** have developed Model Predictive Control (MPC) to SRM drives demonstrating strong capability to handle non-linearities, constraints and multiple-objective handling. Nevertheless, requires high accurate models, substantial computational power, exhibits parameter sensitivity and limiting widespread deployment.

Research Gaps:

Existing SRM improvement techniques including SiC-based converters, multi-level modular converters, QZS converters, DTC with sliding mode observers, fuzzy IITC, and MPC provides only have partial improvements. They still suffer from such as bulky hardware, circuit complexity, increased cost, computational burden, sensitivity to parameter variations, and difficulty in real-time implementation. Besides, these methods also have common problems of torque ripple, nonlinear magnetization, poor speed regulation, and limited adaptability under dynamic operating conditions. The present study combines a simplified (n+1) semiconductor and (n+1) diode converter, hysteresis current-controlled PWM, and an adaptive CRNN controller to achieve low torque ripple, accurate speed control, and efficient real-time operation, thereby overcoming these limitations.

B. Motivation

Predictive Control (PC) is highly suitable for nonlinear systems with constraints and offers significant advantages over conventional control methods. However, traditional PC approaches including generalized, deadbeat, and hysteresis predictive control typically handle only single-objective optimization and are less effective for complex SRM drives. Their performance relies heavily on accurate motor parameters, and conventional analytical models often introduce errors under dynamic conditions.

Existing predictive current-control methods primarily aim to reduce torque ripple and acoustic noise but struggle with inductance variation, dynamic reference currents, and poor low-speed performance. In addition, traditional PC methods produce considerable torque and flux ripple due to inaccurate inductance estimation, ineffective voltage vector selection, and suboptimal sector partitioning.

To overcome these limitations, this research proposes a CRNN integrated with hysteresis current-controlled PWM. The RNN adaptively learns nonlinear SRM dynamics, while the hysteresis PWM provides fast response and consistent current behaviour, enabling effective torque ripple reduction, efficient operation, and

accurate speed regulation. The contributions of the work are,

- The (n+1) semiconductor and (n+1) diode power converter efficiently transfer power from the DC power supply to the SRM with controlled voltage and current to allow for smooth and reliable motor operation.
- Hysteresis current controlled PWM regulates the SRM current phases by maintaining within a predefined hysteresis band, accurately tracking the currents, minimizing overshoot and torque ripple.
- CRNN controller implement to predict the motor's dynamic response based upon previous and present states, adjusting the control signal in real-time and minimize error between reference speed and actual speed for accurate and adaptive speed regulation.
- SRM is employed for its straightforward design, robustness, reliability, and effectiveness over a wide range of speed.

Paper is structured in the following manner: Section II describes circuit design and implementation of the detail working principle. Section III describes modelling of proposed converter, hysteresis current controlled PWM, CRNN, control system for SRM, Section IV provides simulation results, focusing on reduction overall torque ripple, current tracking and speed regulation and a comparative control result against conventional methods. Lastly, Section V provides the conclusion with an overview of the outcomes and contributions of the proposed control approach.

II. PROPOSED MODEL DESCRIPTION

Proposed system utilizes a DC supply as input power for (n+1) semiconductor and (n+1) diode power converter. The power converter topology delivers the ease and energy efficiency of the multilevel converter, lower switching losses, and more reliable commutation of current for the SRM's phases while providing better freewheeling and demagnetization paths.

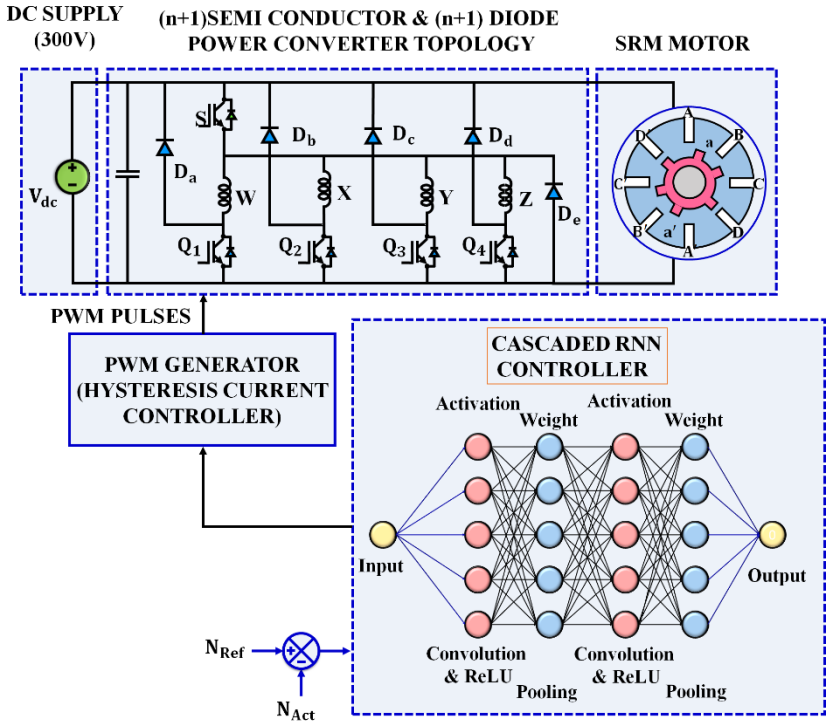

Fig. 1. Proposed block diagram for SRM drives system.

A hysteresis current-controlled PWM generator is used to produce required switching pulses. It maintains motor current in a distinct hysteresis band producing the PWM pulse width signal based on the current-controlled feedback. The current-controlled signals are served to CRNN controller that minimizing the error between reference speed and actual motor speed, thus enabling RNN to adapt to varying conditions. Finally, the controlled pulses are used to drive the SRM, ensuring speed control accuracy and reliable speed stability across operational ranges

of drive system. Fig. 1 illustrates block diagram for the working principle of SRM drive system.

III. PROPOSED METHODOLOGY

A. (n+1) Semiconductor and (n+1) DIODE Power Converter

Proposed converter output power is supplied to SRM through a (n+1) semiconductor and (n+1) diode power converter configuration. This converter is effectively valuable as it reduces the number of semiconductor devices, which minimize the total cost and power losses due to heating effects, while providing a reliable and disturbance free process of complete system. In this configuration, switches and diodes relatively low voltage rating, which improves efficiency and makes the design simpler. The converter as displays in Fig. 2, includes a total of five diodes $(D_a, D_b, D_c, D_d, D_e)$, four switches (Q_a, Q_b, Q_c, Q_d) and four phase windings (W, X, Y, Z). It is evident that fewer switches and diodes facilitate a decrease of overall size of system and therefore the overall cost. Operational basis of the circuit summarized: when Q and Q_a switches are ON, phase winding W is powered by DC source. When switches are OFF, energy kept in winding W is sent back to the source via diode D_b. When the switches Q and Q_b are ON, phase winding X is drive by DC source, while its stowed energy is served back to mains through diode D_c during the OFF states.

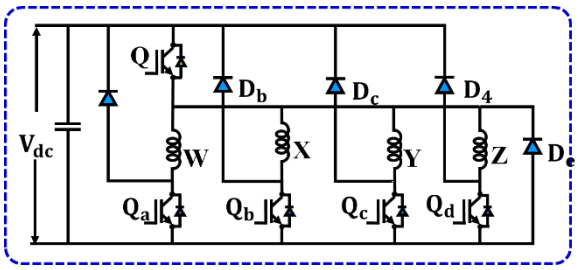

Fig. 2. Proposed converter circuit diagram.

In a similar way, phase winding Y becomes energized when switches Q and Q_c are closed and, when switches are opened, energy is released back to source through diode D_d. Similarly, phase winding Z becomes energized when switches Q and Q_d are closed, and when switches are opened, the energy is again released back to mains through diodeD_e, through the same periodic process of energizing and recovering energy, the converter is actively using power in an efficient manner, subsequently delivering the output to the SRM to serve as its input supply.

B. Hysteresis Current Controller

It's simple and robust control scheme, generally useful in power electronic converters for motor drive systems. This technique constantly evaluates the reference current produced by the controller with the actual motor phase current. The difference between these two currents forms the error signal, which is maintained within a fixed hysteresis band defined by an upper and lower limit. When current error exceed the upper limit, the converter switches are turned ON to reduce error. Conversely, when error exceed the lower limit, the complementary switches are turned ON to increase the current. Fig. 3 and 4 illustrate the hysteresis controller block diagram and the corresponding switching pattern of the hysteresis current waveform.

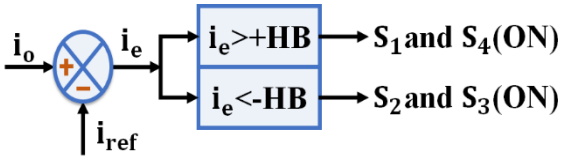

Fig. 3. Sample diagram of Hysteresis controller.

Hysteresis bandwidth h expressed as:

$$h = \frac{V_{dc}^2 - 2(t)^2}{4V_{dc}Ls}, \qquad (1)$$

where, V_{dc} is the voltage of the converter, $e(t)$ is the instantaneous motor back-EMF, L is the motor phase inductance, s is the slope factor.

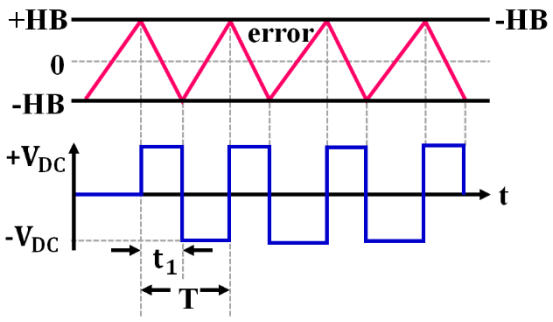

Fig. 4. Hysteresis current controller switching pattern.

The converter switching frequency is determined via a slope of current waveform.

During the interval $0 \to t_1$, when the applied phase voltage is $+V_{dc}$, the ON time written as:

$$t_1 = T_{ON} = \frac{2Lh}{V_{dc} - e(t)}. \quad (2)$$

For the interval $t_1 \to T$, when the phase voltage is $-V_{dc}$, the OFF time expressed as:

$$T - t_1 = T_{OFF} = \frac{2Lh}{V_{dc} - e(t)}. \quad (3)$$

Thus, the total switching period is given by:

$$T = T_{ON} + T_{OFF}, \quad f_{sw} = \frac{1}{T}. \quad (4)$$

Here f_{sw} is the instantaneous switching frequency of the converter. In this motor drive application, the reference current is attained from torque or speed control loop, while the measured current corresponds to the motor phase current. It dynamically regulates motor current within the hysteresis band, enabling fast current response, reduced ripple, and robust motor performance under varying load conditions.

C. Cascaded RNN Controller

A CRNN controller is a control system comprising a series or interconnected RNNs in a hierarchical or sequential structure as shown in Fig. 5. The hierarchical structure allows the controller to manage complex, dynamic systems by solving the problems as interconnected tasks. A primary RNN implements the high- level objectives while the secondary RNNs build the low-level details. The structure of the CRNN controller allows for greater performance, more stable and efficient operation. The CRNN controller that represent both local error dynamics and long-term temporal dependencies of the controlled system.

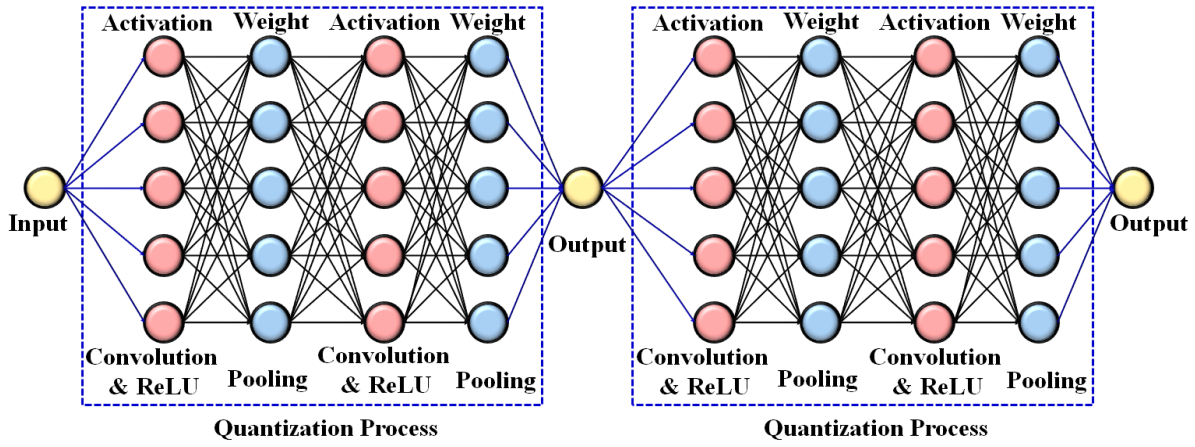

Fig. 5. Structure of CRNN controller.

Let the system error at time t be a given quantity as,

$$e_t = r_t - y_t \quad . \quad (5)$$

Where r_t is the reference input and y_t is the output of the system. The CRNN process the error signal and error history to produce the control signal u_t. The first recurrent layer takes the input error signal and past feedback error signals and gives a hidden state representation with short-term emphasis on error variations:

$$h_t^{(1)} = \phi\left(W^{(1)} e_t + U^{(1)} h_{t-1}^{(1)} + b^{(1)}\right). \quad (6)$$

Here, $h_t^{(1)} \in \mathbb{R}^{H_1}$ is the hidden state vector. $W^{(1)}$ *and* $U^{(1)}$ are weight matrices for error input and recurrent feedback and $b^{(1)}$ stands bias. The activation function $\phi(.)$ introduces non-linearities that allow the controller to deal with non-linear system dynamics. Hence, the output sequence to this stage is given as:

$$F^{(1)} = \left\{h_1^{(1)}, h_2^{(1)}, \ldots, h_T^{(1)}\right\} \quad . \quad (7)$$

This time scale is mainly concerned with temporary error fluctuations. The second recurrent layer improves upon the first-stage features and captures long-term temporal patterns of the error signal with the state evolution described by

$$h_t^{(2)} = \phi\left(W^{(2)} h_t^{(1)} + U^{(2)} h_{t-1}^{(2)} + b^{(2)}\right). \quad (8)$$

Where $h_t^{(2)} \in \mathbb{R}^{H_2}$ is the higher-level hidden state, and $W^{(2)}, U^{(2)}$ *and* $b^{(2)}$ are all trainable parameters. The cascaded feature sequence is,

$$F^{(2)} = \left\{h_1^{(2)}, h_2^{(2)}, \ldots, h_T^{(2)}\right\} . \quad (9)$$

This stage helps the controller incorporate both immediate error corrections and long-term stability in mind. Finally, the control input u_t that is applied to the plant is calculated as either a linear or nonlinear mapping of the cascaded hidden state.

$$u_t = Vh_t^{(2)} + c \ . \quad (10)$$

Where V denotes output weight matrix and c stands output bias. This ensure that the control signal generated depend on both current error and its past dynamics, as encoded into the CRNN layers.

D. Modelling of SRM

The continually evolving computational representation of an SRM is essential for implementing the proposed CRNN approaches. SRM has double salient pole nonlinear behaviour and is a multivariate system. It's primary design is shown in Fig. 6. The written formula of SRM drive structure is as follows:

$$V = i \times R_s + \frac{d\lambda(\theta, i)}{dt} . \quad (11)$$

Here, R_s stands stator resistance, λ denotes flux linkage, θ *and* i denotes rotor position and stator phase current, respectively. Function of flux linkage is connected with phase current and rotor position, as given in the formula,

$$V = i \times R_s + \frac{\partial\lambda}{\partial\theta}\frac{d\theta}{dt} + \frac{\partial\lambda}{\partial i}\frac{di}{dt} . \quad (12)$$

The nonlinear relationship of flux linkage, which is expressed in degrees of angle with phase winding current and rotor position, technically includes three regions: aligned, unaligned, and partially aligned states as discussed in the analytical model for estimating phase current as stated in equation (13).

$$\frac{di}{dt} = \frac{1}{\frac{\partial\lambda}{\partial i}}\left(v - R_s i - \frac{\partial\lambda}{\partial\theta}\omega\right). \quad (13)$$

In this equation, ω stands angular velocity. The stator phase current varies as a function of rotor position $\lambda(\theta, i)$. Instantaneous electromagnetic torque is derived directly from the co-energy–based mathematical formulation. Also, the torque generated from a single phase is equal to the torque produced from the motor represented in equation (14),

$$T_{ph}(i, \theta) = \frac{\partial w_c}{\partial\theta} . \quad (14)$$

Where equation (15), w_c co-energy stands stated as:

$$w_c = \int_0^i \lambda(i, \theta)\, di . \quad (15)$$

The equation (16) total torque established is stated as:

$$T_e = \sum T_{ph}(i, \theta) = j\frac{d\omega}{dt} + B\omega + T_L . \quad (16)$$

Here, T_e: electromagnetic torque; T_{ph}: torque per phase j: moment of inertia; B : damping factor; ω: rotor speed and T_L: load torque. It is observed that when rotor is placed in an aligned position, the unsaturated inductance increases, whereas it achieves its minimum when it's placed in the unaligned position.

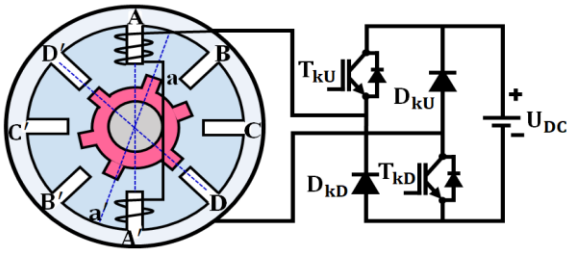

Fig. 6. Structure of SRM.

Let equations (17-18) represent the magnetisation properties of the SRM flux linkage and torque modelling equation.

$$\lambda(i, \theta) = L_c i + \left[L_b i + A\left(1 - e^{-Bi}\right) - L_c i\right] f(\theta) , \quad (17)$$

$$T_{ph} = \left[\frac{L_b - L_c}{2} i^2 + Ai - \frac{A}{B}\left(1 - e^{-Bi}\right)\right] f(\theta) . \quad (18)$$

In the SRM inductance attributes magnetisation curve, L_b represents aligned position's saturated inductance, L_c indicates unaligned position's inductance, and L_d indicates possible aligned position's saturated inductance. H ere an equation is used to denote the values of A *and* B ,

$$A = \lambda_m - L_b i_m \quad (19)$$

$$B = \left(L_d - L_b\right) / \left(\lambda_m - L_b i_m\right) \quad (20)$$

$$f\left(\theta\right) = \left(2N_r^2 / \pi^3\right)\theta^3 - \left(\frac{2N_r^2}{\pi^2}\right)\theta^2 + 1 \quad (21)$$

Here $f\left(\theta\right)$ indicates the magnetisation curves' intermediate locations are generated by interpolating two external curves, $A and B$ are selected consistent as a function of rated current (I_m) with regard to matching flux linkage, and N_r indicates a number of rotor poles. The mathematical models for the behaviour of SRM have been summarised as follows:

$$\frac{di}{dt} = \frac{1}{\frac{\partial \lambda_p}{\partial i}}\left(v - R_s i - \frac{\partial \lambda_p}{\partial \theta}\omega\right), \left[p = 1,2,3,4\right] \quad (22)$$

$$\frac{d\omega}{dt} = \frac{1}{j}\left[T_e - T_L - B\omega\right] \quad (23)$$

$$\frac{d\theta}{dt} = \omega, \theta_p = \theta - \left(p-1\right)\pi / 3 \quad (24)$$

SRM is well-known for its simple construction, high efficiency, extended speed range of operation, and generally dependable performance for many drive applications. In addition, fault tolerance. high torque density, and low maintenance make the SRM a viable option for electric vehicles and industrial systems.

IV. RESULT AND DISCUSSION

The presented system includes a (n+1) semiconductor and (n+1) diode power converter, hysteresis current-controlled PWM, and CRNN controller, simulated and tested via MATLAB/Simulink. Performance results are shown in terms of current tracking, torque ripple reduction, and speed regulation performance of the SRM drive. These are compared to conventional techniques to demonstrate the advantages of the proposed strategy. Table 1 illustrates proposed parameter specifications.

Table 1 Parameter Specifications

Parameter	Specifications
DC Source	
DC Source Voltage	$600V$
SRM Drive	
Speed	$2000 rpm$
$Load\ inertia\left(J\right)$	$9\times10^{-4}\ Nm^2$

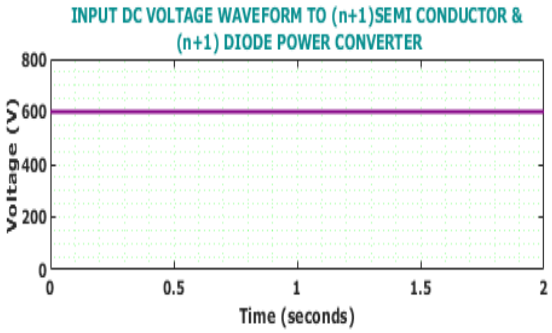

Fig. 7. Input DC voltage waveform.

Fig. 7 illustrates input DC voltage waveform applied to the proposed converter. Constant DC voltage of $600V$ is maintained throughout the simulation period thus assuring a stable input source to SRM drive. A stable supply input ensures a consistent operation of the converter and consistent performance of motor under various changing conditions.

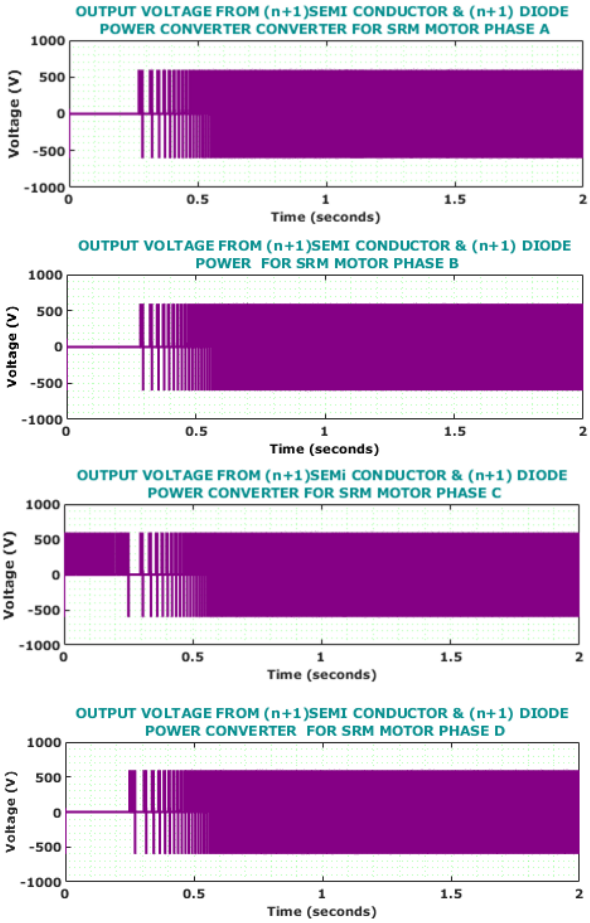

Fig. 8. Output voltage from converter for SRM motor phases.

Fig. 8 shows proposed converter output voltage waveforms for the four phases of SRM drive. In Phase A, the converter produces bipolar

voltage pulses switching between $\pm 600V$ to deliver the proper excitation of the winding. In Phase B, controlled voltage pulses of the same amplitude are applied to provide appropriate commutation and achieve proper phase displacement. Phase C applies controlled bipolar pulses $(\pm 600V)$ in a regulated manner to maintain the excitation and deliver torque; and Phase D shows properly excited with the same bipolar voltage swings, completing the four-phase drive. Even with these individual voltages, the results indicate that the proposed converter deliver uniform and accurate excitation across all phases of the SRM, along with stable torque production and reliable drive operation.

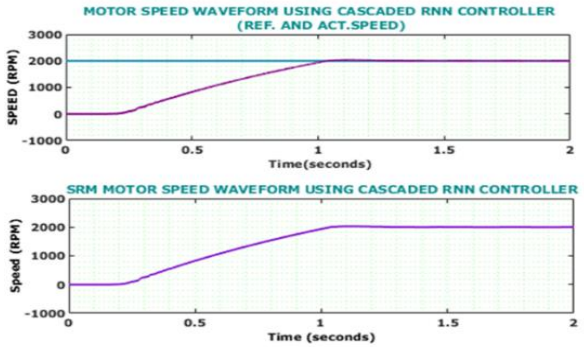

Fig. 9. Motor speed waveform of the SRM drive using CRNN controller.

Fig. 9 shows speeds of motor tracked by the CRNN controller, where reference speed and actual speed are compared.

The initial motor speed started from rest zero and accelerated very quickly by achieving the reference speed. After about 1s, the motor reached a steady-state speed of 2000 RPM with a near steady-state error.

This experiment confirms the ability of the proposed controller to achieve proper speed regulation and offer steady dynamic performance of the SRM drive. Fig. 10 show flux and current responses of the SRM motor.

The flux is stable at $0.15Wb$, although with some initial transient overshoots. The current waveforms show phase currents rising to $20-25A$ with controlled switching and controllable transient overshoot to ensure smoother excitation of the motor phases. The results indicate an effective management of flux linkage with a low level of current distortion under the proposed control strategy.

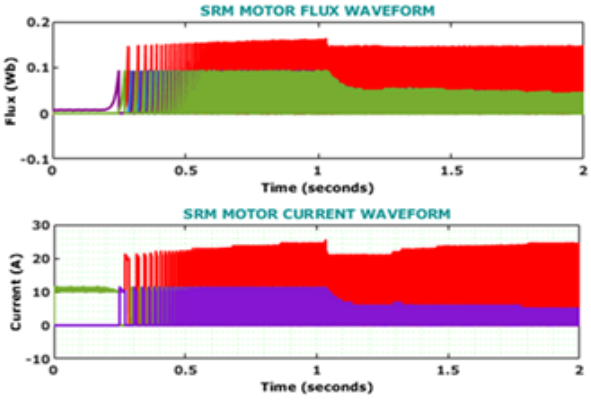

Fig. 10. Flux and current waveforms of the SRM.

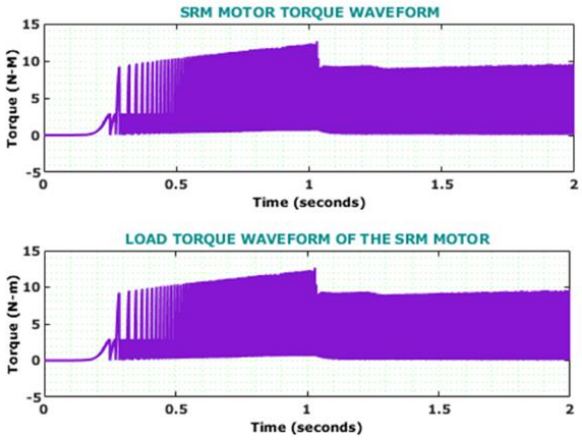

Fig. 11. Torque and load torque waveforms of the SRM.

Fig. 11 illustrates the developed torque and load torque characteristics of the SRM motor. The torque increases and stabilizes at $5-10\,Nm$, with appreciable reductions in torque ripple after 1s. The load torque follows a similar trend to the developed torque confirming the effective tracking capability. This confirms that the CRNN controller reduces torque ripple, providing more stability and performance of drive system.

Fig. 12 represents torque ripple performance of the proposed CRNN–hysteresis PWM-based SRM drive is compared with the established methods reported in Ref. [15], Ref. [22], and Ref. [23]. The proposed system is clearly able to achieve lower torque ripple in the speed range (200–2000 rpm) across the speed range than the other methods. The torque flux ratio across different speeds, from which it is shown that the proposed method achieves a greater torque-to-current ratio in all conditions compared to the other methods, which suggests that it is more efficient and is making better use of the current.

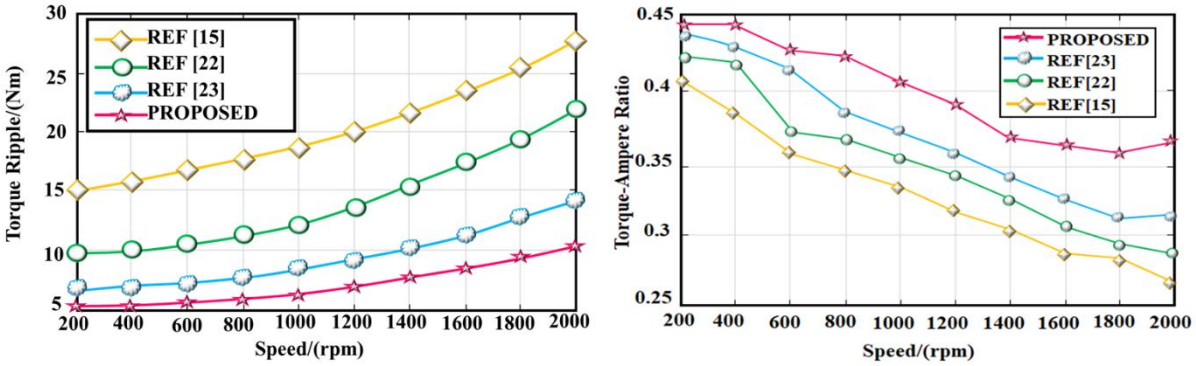

Fig. 12. Comparison of torque ripple and torque flux for different methods.

Table 2

Comparison of settling time and rise time for controller

Controllers	Settling Time (t_s)	Rise Time (t_r)
REF [24]	2.75s	1.53s
REF [25]	0.08s	0.094s
PROPOSED	0.06	0.03s

Table 2 illustrates comparison of transient performance of the proposed CRNN–hysteresis PWM controller with classical controllers in Ref. [24] and Ref. [25]. The proposed controller has the fastest response with a settling time of 0.06 s and rise time of 0.03 s, which is substantially faster than the reported methods. This indicates proposed control strategy's ability to regulate speed in SRM drives to a greater extent than the referenced methods.

V. CONCLUSION

The proposed SRM drive system effectively integrates (n+1) semiconductor and (n+1) diode power converter and an intelligent control strategy. The proposed converter minimizes the number of devices, switching losses, and low system cost while providing smooth commutation characteristics, and reliable power delivery.

With the aid of hysteresis current controlled PWM with CRNN achieved precise current tracking, large reduction in torque ripple performance and accurate real-time speed tracking, despite operating in dynamic conditions.

The results of the simulations carried out with MATLAB/Simulink have demonstrated that this system offers improved speed of response, steady state performance, and robustness in comparison to conventional methods. Therefore, combination of the simplified converter and the adaptive controller makes proposed SRM drive ideal for next-generation electric vehicle and industrial drives that certainly need to be efficient, reliable and cost effective.

REFERENCE

[1] Shahapure S.B., Kulkarni V.A., Shinde S.M. A Technology Review of Energy Storage Systems, Battery Charging Methods and Market Analysis of EV Based on Electric Drives. *Development*, 2022, vol. 6, no. 8.

[2] Kavin K.S., Karuvelam P.S., Pathak A., Premila T.R., Hemalatha R., Kumar T. Modelling and analysis of hybrid fuzzy tuned PI controller based PMBLDC motor for electric vehicle applications. *SSRG International Journal of Electrical and Electronics Engineering*, 2023, vol. 10, no. 2, pp. 8-18.

[3] El Hadraoui H., Zegrari M., Chebak A., Laayati O., Guennouni N. A multi-criteria analysis and trends of electric motors for electric vehicles. *World Electric Vehicle Journal*, 2022, vol. 13, no. 4, pp. 65. https://doi.org/10.3390/wevj13040065 .

[4] Zhou C., Huang X., Li Z., Cao W. Design consideration of fractional slot concentrated winding interior permanent magnet synchronous motor for EV and HEV applications. *IEEE Access*, 2021, vol. 9, pp. 64116-64126. https://doi.org/10.1109/ACCESS.2021.3073743 .

[5] Prabhu M.A., Sheela G.E., Alzahrani H., Siddiq H., Okmi A., Alharbi N., Florence, S.S., Lekshmy M.S., Velayuthan Pillai S. Green synthesis of ZnO, Fe3O4, and TiO2 nanoparticles: exploring enhanced bacterial inhibition, catalysis, and photocatalysis for sustainable environmental applications. *International Journal of Environmental Analytical Chemistry*, 2024, pp. 1-25. https://doi.org/10.1080/03067319.2024.2404533.

[6] Salahuddin H., Imdad K., Chaudhry M.U., Nazarenko D., Bolshev V., Yasir, M. Induction

machine-based EV vector control model using Mamdani fuzzy logic controller. *Applied Sciences*, 2022, vol. 12, no. 9, pp. 4647. https://doi.org/10.3390/app12094647 .

[7] Smonia Joe Princy S., Hentry C., Alharbi N., Siddiq H., Refaei M., Alzahrani H., Bindhu M.R., Sarojini V., Sasi Florence S. Synergistic Antimicrobial and Photocatalytic Properties of PVP-Ag-PEG Nanocomposites for Sustainable Leachate Treatment. *Journal of Inorganic and Organometallic Polymers and Materials*, 2024, pp. 1-19. https://doi.org/10.1007/s10904-024-03490-w .

[8] Priya A.K. Enhancement of VANETS Security against Gray Hole Attack with ANFIS-GWO and LBK. *International Journal of Advanced Trends in Engineering and Management (IJATEM)*, 2024, vol. 03, no. 04, pp. 31-40.

[9] Ali T.F., Dominic D.A., Prabhakaran P. A systematic approach to digital control development for four-phase srm drive using single current sensor for medium power applications. *IEEE Access*, 2024, 12, pp. 34074-34088. https://doi.org/10.1109/ACCESS.2024.3372988 .

[10] Kumarasabapathy N., Kavin K.S., Sakthidhasan K., Martin G.W., Gr S. Nadu T. Optimized Speed and Current Controller Based High Speed Switched Reluctance Motor for EV Applications.

[11] Abhijith V., Hossain M.J., Lei G., Sreelekha P.A., Monichan T.P., Rao S.V. Hybrid switched reluctance motors for electric vehicle applications with high torque capability without permanent magnet. *Energies*, 2022, vol. 15, no. 21, pp. 7931. https://doi.org/10.3390/en15217931 .

[12] Kumar P., Israyelu M., Sashidhar S. A simple four-phase switched reluctance motor drive for ceiling fan applications. *IEEe Access*, 2023, vol. 11, pp. 7021-7030. https://doi.org/10.1109/ACCESS.2023.3238068 .

[13] Faizal A.M., Maheswari E., Raviteja P., Kavin K.S., Chithra S., Gayathri A.R. Improved Boost Converter for Solar System in Grid Connected EV Charging Station. In *2024 International Conference on Recent Advances in Electrical, Electronics, Ubiquitous Communication, and Computational Intelligence (RAEEUCCI)*, 2024, pp. 1-6. IEEE. https://doi.org/10.1109/RAEEUCCI61380.2024.10547918 .

[14] Pawar J.D., Nikose M.D. Control of Torque Ripple and Rotor Position for SRM (8/6-4 Phases) Using an Optimization-Based Model Predictive Torque Control. *Advanced Control for Applications: Engineering and Industrial Systems*, 2025, vol. 7, no. 1, pp. e242. https://doi.org/10.1002/adc2.242 .

[15] Ali T.F., Dominic D.A., Prabhakaran P., Parameswaran A.P. A bidirectional interleaved totem pole PFC-based integrated on-board charger for EV SRM drive. *IEEE Access*, 2024. https://doi.org/10.1109/ACCESS.2024.3432791 .

[16] Juarez-Leon, F., Bilgin, B. A High-Efficiency Silicon-Carbide Bidirectional Industrial Switched Reluctance Motor Drive. *IEEE Access*, 2025, vol. 13, pp. 126513 - 126524. https://doi.org/10.1109/ACCESS.2025.3590302 .

[17] Malekpour H., Rashidi A., Nejad S.M.S., Lee D.H. Multi-Level Voltage High Fault-Tolerance Modular SRM Converter with Simultaneous Charge and Discharge Capability for HEV. *IEEE Access*, 2025, vol. 13, pp. 127447 - 127461. https://doi.org/10.1109/ACCESS.2025.3587508 .

[18] Sun Q., Chen L., Liu X., Niu F., Gan C. Quasi-Z-source-fed SRM drive for torque ripple minimization and speed range extension with three-switch conduction. *IEEE Transactions on Industrial Electronics*, 2023, vol. 70, no. 12, pp. 11923-11933. https://doi.org/10.1109/TIE.2022.3232653.

[19] Sun X., Wu J., Lei G., Guo Y., Zhu J. Torque ripple reduction of SRM drive using improved direct torque control with sliding mode controller and observer. *IEEE Transactions on Industrial Electronics*, 2020, vol. 68, no. 10, pp. 9334-9345. https://doi.org/10.1109/TIE.2020.3020026 .

[20] Jing B., Dang X., Liu Z., Long S. Torque ripple suppression of switched reluctance motor based on fuzzy indirect instant torque control. *IEEE Access*, 2022, vol. 10, pp. 75472-75481. https://doi.org/10.1109/ACCESS.2022.3190082 .

[21] Valencia D.F., Tarvirdilu-Asl R., Garcia, C., Rodriguez J., Emadi A. Vision, challenges, and future trends of model predictive control in switched reluctance motor drives. *IEEE Access*, 2021, vol. 9, pp. 69926-69937. https://doi.org/10.1109/ACCESS.2021.3078366 .

[22] Thirumalasetty M., Narayanan G. High-Performance Torque Controller for Switched Reluctance Machine. *IEEE Transactions on Industry Applications*, 2024, vol. 60, no. 5, pp. 6923-6937. https://doi.org/10.1109/TIA.2024.3403974 .

[23] Pushparajesh V., Nandish B.M., Marulasiddappa H.B. Hybrid intelligent controller based torque ripple minimization in switched reluctance motor drive. *Bulletin of Electrical Engineering and Informatics*, 2021, vol. 10, no. 3, pp. 1193-1203. https://doi.org/10.11591/eei.v10i3.3039 .

[24] Alqahtani S., Ganesan S., Zohdy M.A. The comparison between PI and PID controllers in engine speed control model. *In 2020 IEEE International Conference on Electro Information Technology (EIT)*, 2020, pp. 629-634. IEEE. https://doi.org/10.1109/EIT48999.2020.9208313 .

[25] Kanungo A., Choubey C., Gupta V., Kumar P., Kumar N. Design of an intelligent wavelet-based fuzzy adaptive PID control for brushless motor. *Multimedia Tools and Applications*, 2023, vol. 82, no. 21, pp. 33203-33223. https://doi.org/10.1007/s11042-023-14872-6.

Information about authors.

Saritha Kandukuri is the Master of Engineering in High Voltage Power Systems at Godavari Institute of Engineering and Technology, Rajahmundry, Andhra Pradesh, India. Scientific interests: power systems and renewable energy systems.
E-mail: mugatha.saritha@gmail.com
ORCID: https://orcid.org/0000-0002-6700-1134

Garaboyina Mohitha Sree is UG research scholar.
Scientific interests: power systems and renewable energy systems.
Email: gsudha7095@gmail.com
ORCID: https://orcid.org/0009-0008-7899-9623

Gopal Kumar is UG research scholar. Scientific interests: power systems and renewable energy systems.
Email: gopal.godavari2022@gmail.com
ORCID: https://orcid.org/0009-0007-6837-3080

Sivaprasad Kollati is a Research Scholar, pursuing Ph.D., in Electrical Engineering at Andhra University, Visakhapatnam, Andhra Pradesh, India. His main area of interest includes Power Electronic and Renewable Energy Systems.
Email: ksivaprasad22@gmail.com
ORCID: https://orcid.org/0000-0002-7170-7316

Ankit Raj is UG research scholar.
Scientific interests: power systems and renewable energy systems.
Email: Ankitatraj808495@gmail.com
ORCID: https://orcid.org/0009-0006-7184-9476